

Ghost Imaging with Different Speckle Sizes of Thermal Light

Jue Wang, Renlong Yu, Yu Xin*, Yanming Shao, Yanru Chen, and Qi Zhao

Department of Optical Engineering, Nanjing University of Science and Technology, Nanjing 210094, China

(Received September 17, 2015 : revised December 8, 2015 : accepted December 21, 2015)

In this paper, we theoretically and experimentally analyze the impact of speckle size of pseudo-thermal light source on ghost imaging. A larger size of speckle can bring improvements in SNR and visibility. At the same time, the edge blur of the retrieved image will become more serious. We also present a setup which can mitigate the edge blur of larger speckle while maintaining the advantages of higher SNR and visibility by changing the speckle size of the object beam with a concave lens.

Keywords : Ghost imaging, Coherence, Speckle size, Edge blur

OCIS codes : (030.0030) Coherence and statistical optics; (030.6600) Statistical optics; (110.6820) Thermal imaging

I. INTRODUCTION

In the past decade, ghost imaging (GI) has attracted a lot of attention. In ghost imaging, the object image is retrieved by using two spatially correlated beams: the reference beam and the object beam. The reference beam never interacts with the object and is measured with a pixelated detector. The object beam interrogates the object and then illuminates a bucket detector, with no spatial resolution. By correlating the reference beam with the bucket signal, the ‘ghost’ image is retrieved. In 1995, the first GI was found in quantum optics [1], and it was once considered as a unique phenomenon of quantum optics. However, in 2002, Bennink achieved ghost imaging with scanning of a pair of collimated laser beams [2], which sparked a debate [3-5] of whether GI was a quantum effect or not. Then a variety of thermal light sources [3-8] were used to realize GI. Recently some teams focused on the application of GI, such as GI by measuring reflected photons [9], compressive GI [10-12], GI through turbulent atmosphere [13], GI in turbid media [14]. However, only a few teams [7, 15, 16] focused on the impact of the speckle size on GI. In this paper, we theoretically and experimentally analyze the pros and cons of GI with different speckle sizes, and try to present a setup which can at the same time make the best use of the advantages and bypass the disadvantages caused by different sizes of speckles.

II. METHODS & RESULTS

In order to get speckles with different sizes, we used the setup in [17] (see Fig. 1(a)). The laser and rotating

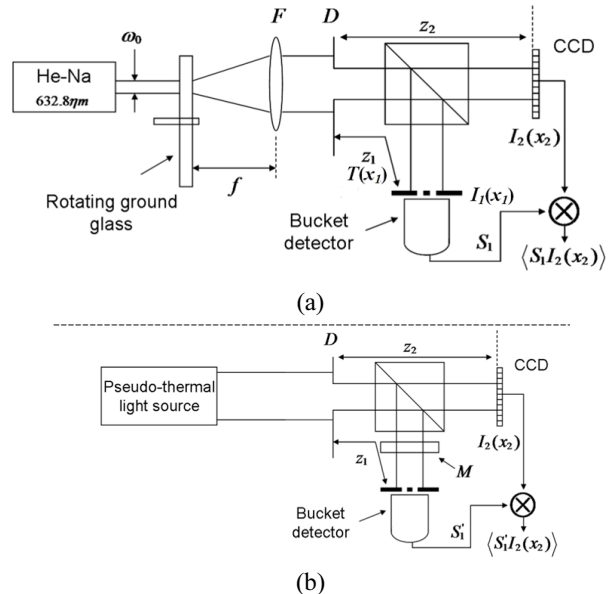


FIG. 1. Experimental setups for ghost imaging. (a) the traditional setup for ghost imaging. (b) the improved setup for ghost imaging.

*Corresponding author: yxin@njust.edu.cn

Color versions of one or more of the figures in this paper are available online.

ground glass constituted a pseudo-thermal light source. The ground glass was in the focal plane of the Lens F while D was an aperture. With the formula $\delta x_0 = \pi \lambda f / \omega_0$, we can get desired speckle size δx_0 by changing f of Lens. Here, λ is the wavelength of light and ω_0 represents the waist radius. The role of beam splitter is to form two spatially correlated beams. Beam 1 (the object beam) is collected with a bucket detector after illuminating the object. Beam 2 (the reference beam) never interacts with the object and measured with a pixelated detector. The distance between Aperture D and the two detectors are z_1 and z_2 respectively. Let us indicate with $I_1(x_1)$ and $I_2(x_2)$, the intensity distributions of the speckle fields on the object and reference planes, respectively. If $T(x)$ indicates the transmission function, the bucket signal S_1 is

$$S_1 = \int I_1(x_1) |T(x_1)|^2 dx_1 \quad (1)$$

According to the result of [7], we have the following formula

$$\nu_{\Delta z}(x_2) \equiv \frac{\langle \delta S_1 \delta I_2(x_2) \rangle}{\langle S_1 \rangle \langle I_2(x_2) \rangle} = \frac{|T(x_2)|^2 \otimes \gamma_{\Delta z}(x_2)}{N_{obj}} \quad (2)$$

$$\gamma_{\Delta z}(x) = \frac{|\mu_{\Delta z}(x)|^2}{\int |\mu_{\Delta z}(x)|^2 dx} = \frac{|\mu_{\Delta z}(x)|^2}{A_{coh}} \quad (3)$$

Where $\langle \dots \rangle$ indicates the average over independent speckle configurations. $\mu_{\Delta z}(x_1, x_2)$ is the cross-correlation coefficient of the electric fields at the planes z_1 and z_2 . A_{coh} is the area of the speckle, which is related to the speckle size by $\delta x_0 = \sqrt{A_{coh}}$. \otimes denotes convolution, $N_{obj} = A_{obj} / A_{coh}$ denotes the number of the speckles falling into the object. Eq. (2) shows that the visibility of GI [i.e., the maximum value of $\nu_{\Delta z}(x_2)$] is equal to $1/N_{obj}$ and, except for convolution effects (occurring when $\gamma_{\Delta z}(x_2, x_1)$ and $T(x_2, x_1)$ have similar widths), is independent of Δz . Another indicator to evaluate the GI is SNR [15, 16]

$$SNR = \frac{R}{N_{speckle}} \frac{\Delta T_{min}^2}{T^2} \quad (4)$$

While $N_{speckle} = A_{beam} / A_{coh}$ is the number of the speckles in the beam, ΔT_{min} is the minimum variation of the object transmission function to be detected. $\overline{T^2} = \int_{A_{beam}} \langle I(x) \rangle$ $T^2(x) d^2x / \int_{A_{beam}} \langle I(x) \rangle d^2x \approx \int_{A_{beam}} T^2(x) d^2x / A_{beam}$ is the average quadratic transmission function of the object. R represents the independent sampling number. With Eqs. (2) and (4), we know that for the case of using the same average number, a larger speckle size will lead to higher

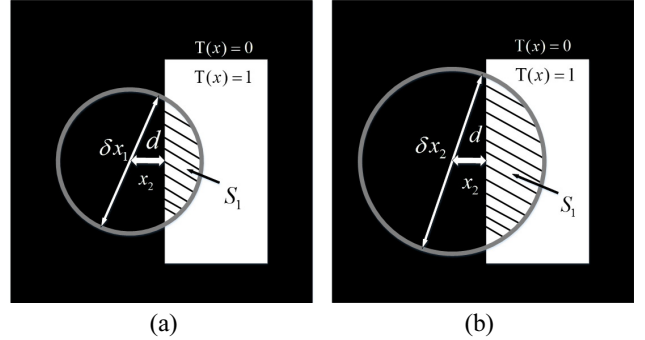


FIG. 2. The schematic view of the point x_2 where the transmission function is $T(x_2) = 0$.

visibility and SNR. However, in experiments we found that a larger speckle size will get a more blurred edge of the object as well. We call this phenomenon edge blur of GI. We will theoretically analyze the reason of this phenomenon and experimentally show the edge blur of GI in the following.

Considering the case shown in Fig. 2, there is a point x_2 where the transmission function is $T(x_2) = 0$, and the distance from the edge is d . δx_1 and δx_2 are the sizes of two different speckles where $\delta x_1 < \delta x_2$. The shaded areas indicate that the region can be received by the bucket detector. When $\delta x_0 = D$, the mutual coherence function [18] is

$$G^{(1)}(x_1, 0; x_2, 0) = I_0 \left(\frac{x_1 + x_2}{2} \right) C_0(x_2 - x_1) \quad (5)$$

Where I_0 is a real function representing the mean transverse intensity distribution at the source plane, varying on the large scale D the source diameter. C_0 is a real function with the property $C_0(0) = 1$, which dies out over the small scale δx_0 (the speckle transverse size). In the deep-Fresnel zone, the coherence factor characterizing the granular structure of the source has a Gaussian profile of the form

$$C_0(x_2 - x_1) = \exp \left[-\frac{|x_2 - x_1|^2}{\delta x_0^2} \right] \quad (6)$$

Here, we only consider the case $z_1 = z_2$. Then, we obtain the complex coherence factor and its squared modulus reads as:

$$|\mu_0(x_2 - x_1)|^2 = \exp \left[-\frac{2|x_2 - x_1|^2}{\delta x_0^2} \right] \quad (7)$$

Eq. (7) illustrates that in the case where $z_1 = z_2$, $|\mu|^2$ is a Gaussian function described by the size δx_0 . The graph

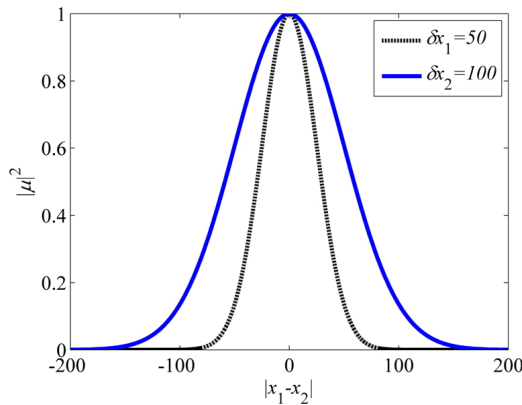


FIG. 3. The graph of $|\mu|^2$ vs $|x_1 - x_2|$.

of $|\mu|^2$ and $|x_1 - x_2|$ is shown in Fig. 3. We can see that for the same $|x_1 - x_2|$, a larger speckle leads to a bigger $|\mu|^2$.

The correlation between S_1 and $I_2(x_2)$ is

$$\langle SI_2(x_2) \rangle = \left\langle I_2(x_2) \int_{beam} I_1(x_1) |T(x_1)|^2 dx_1 \right\rangle \quad (8)$$

Assuming that the bucket detector is pixelated, so we obtain discrete result

$$\langle SI_2(x_2) \rangle = \sum_{i=1}^N \langle I_1(x_{1i}) I_2(x_2) \rangle \quad (9)$$

$$\begin{aligned} & \langle I_1(x_1) I_2(x_2) \rangle \\ &= \langle I_1(x_1) \rangle \langle I_2(x_2) \rangle [1 + |\mu_0(x_2 - x_1)|^2] \end{aligned} \quad (10)$$

Where N denotes the number of the pixels in the shaded areas in Fig. 2. From Fig. 3 we can see that

$$|\mu_0(x_2 - x_1)|^2_{\delta x_1} < |\mu_0(x_2 - x_1)|^2_{\delta x_2} \quad (11)$$

Combining Eqs. (10) and (11), we have the result

$$\langle I_1(x_1) I_2(x_2) \rangle_{\delta x_1} < \langle I_1(x_1) I_2(x_2) \rangle_{\delta x_2} \quad (12)$$

On the other hand, from Fig. 2, the number of pixels has the relation that $N_{\delta x_1} < N_{\delta x_2}$, so we obtain the final result

$$\langle SI_2(x_2) \rangle_{\delta x_1} < \langle SI_2(x_2) \rangle_{\delta x_2} \quad (13)$$

Eq. (13) shows two key features of GI with a pseudo-thermal light source: Firstly, because of the Gaussian distribution of the correlation radius of the speckle, $I_2(x_2)$ and bucket signal S_1 are still related and the retrieved $T(x_2) > 0$, although the ideal $T(x_2) = 0$. Theoretically, when $d > \delta x_0 / 2$, the transmission function $T(x_2) = 0$, and we call this distance $\delta x_0 / 2$ as the width of edge blur. Secondly, while Eqs. (2) and (4) illustrate that the ghost imaging will have a higher visibility and SNR with larger speckle, Eq. (13) shows that it will bring a more serious edge blur as well.

In order to experimentally demonstrate the edge blur, we implement the experiment shown in Fig. 1(a). The source is a He-Ne laser ($\lambda = 632.8 \text{ nm}$, $\omega_0 = 2 \text{ mm}$). By selecting different lenses ($f = 50 \text{ mm}$ and $f = 100 \text{ mm}$, respectively), we obtain two kinds of speckle with $\delta x_1 = 49.7 \mu\text{m}$ and $\delta x_2 = 99.4 \mu\text{m}$. The object was an aperture whose diameter is $900 \mu\text{m}$. The experimental result is shown in Fig. 4. Where Panel a1 shows the 2D-ghost image retrieved by averaging $R=12800$ independent realizations of the speckle field ($\delta x_1 \approx 50 \mu\text{m}$). Panel b1 shows the horizontal profile of the aperture (blue continuous line), this profile compares with the expected one (dotted line) and its visibility is 0.0039. Panel a2 shows the 2D-ghost image retrieved by averaging $R = 12800$ independent realizations of the speckle field ($\delta x_2 \approx 100 \mu\text{m}$). Panel b2 shows the horizontal profile of the aperture (blue continuous line), this profile compares with the expected one (dotted line) and its visibility is 0.0156.

Comparing the results with different speckles, we have the following conclusions: Firstly, compared with Fig. 4(a1),

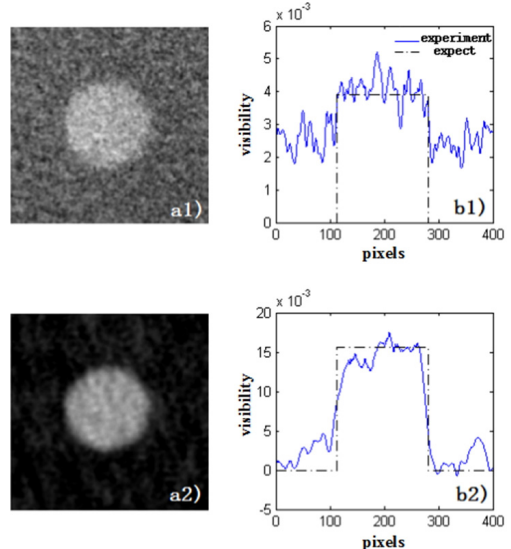


FIG. 4. The ghost imaging reconstruction of an aperture whose diameter is $900 \mu\text{m}$. (a1) and (b1) are the reconstruction images which obtain 12800 realizations, when the speckle size of the thermal source is $50 \mu\text{m}$. (a2) and (b2) are the reconstruction image which obtain 12800 realizations, when the speckle size of the thermal source is $100 \mu\text{m}$.

the retrieved image with larger speckle (see Fig. 4(a2)) has a higher SNR. Secondly, compared with Fig. 4(b1), the retrieved image with larger speckle (see Fig. 4(b2)) has a higher visibility, which is about four times of the visibility retrieved with smaller speckle. Thirdly, compared with Fig. 4(b1), Fig. 4(b2) has a wider rising edge. This shows that the larger speckle used, the more serious edge blur exists.

Based on the analysis above, we try to present a setup (Fig. 1(b)) which can eliminate the adverse effects of speckle size. In Fig. 1(b), the reference beam remains intact, and an optical modulator M is added to the object beam. The M is used to modulate the distribution of the light, and it can be a spatial light modulator (SLM) or lens, simply. Then the bucket signal can be rewritten as

$$S_1 = \int I'_1(x_1) |T(x_1)|^2 dx_1 \quad (14)$$

Where $I'_1(x_1) = mI_1(nx_1)$ represents the modulated light field, m and n are the modulation coefficients. By converting the variable, we have the following result

$$\begin{aligned} S_1 &= mn^{-1} \int I_1(x_1) \left| T\left(\frac{x_1}{n}\right) \right|^2 dx_1 \\ &= mn^{-1} \int I_1(x_1) |T'(x_1)|^2 dx_1 \end{aligned} \quad (15)$$

$$T\left(\frac{x_1}{n}\right) = T'(x_1) \quad (16)$$

The difference between Eq. (1) and Eq. (15) is the transmission function $T'(x)$, which indicates that the modulation of the light is equivalent to the modulation of the object. When $n > 1$, the effect is to narrow the object. When $n < 1$, the effect is to amplify the object. So we have the following formula

$$\begin{aligned} v_{\Delta z}(x_2) &\equiv \frac{\langle \delta S_1' \delta I_2(x_2) \rangle}{\langle S_1' \rangle \langle I_2(x_2) \rangle} \\ &= \frac{|T'(x_2)|^2 \otimes \gamma_{\Delta z}(x_2)}{N_{obj}'} \end{aligned} \quad (17)$$

This setup has at least three advantages: Firstly, we can arbitrarily zoom the object by setting different n . This feature allows us to image an object whose size is larger than the size of the detector. Secondly, according to Eq. (17), when $n > 1 / N_{obj}' > N_{obj}$ which illustrates that the improved setup has a higher visibility than the traditional setup. Thirdly, because the reference beam remains intact, the width of the edge blur remains $\delta x_0 / 2$.

Two independent experiments were implemented with

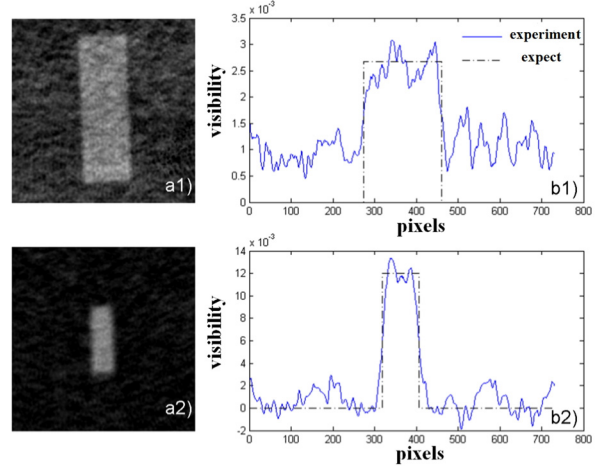


FIG. 5. The ghost imaging reconstruction of a $1 \text{ mm} \times 3 \text{ mm}$ slit. (a1) and (b1) are the reconstruction image of the traditional setup, obtained with 16000 realizations. (a2) and (b2) are the reconstruction image of the improved setup, obtained with 16000 realizations.

the setups shown in Figs. 1(a) and (b), respectively. The two objects have the same size (slit, $1 \text{ mm} \times 3 \text{ mm}$). In Fig. 1(b), we used a concave lens as the modulator M and $n = 2.12$. The results are shown in Fig. 5. Panels a1 and b1 are results of the traditional ghost imaging while Panels a2 and b2 represent results of the improved method. The visibility of results in Panels a1 and b1 is about 0.0026, and the visibility of results in Panel a2 and b2 is about 0.012. We can see the improved ghost imaging has higher SNR and visibility (about 4.5 times) than the traditional ghost imaging by comparing the results. The improvement of visibility is due to the change of modulation coefficient n. Moreover, Panels b1 and b2 show that the two retrieved image have the same width of edge blur. However, there is a price to pay, which is the retrieved image is a narrowed object. The experimental results are in good agreement with the theoretical analysis results.

III. CONCLUSION

In this paper, the impact of speckle size of pseudo-thermal light source on ghost imaging is theoretically and experimentally analyzed. For the same number of independent realizations, the larger speckle size of thermal source is, the higher visibility and SNR of the retrieved image and the more serious edge blur of the retrieved image will be. This means that the impact of the speckle size of the pseudo-thermal on GI is double-sided. In order to eliminate the adverse effects of the speckle size, we use a concave lens to modulate the object beam, which is equivalent to modulating the object. By the improved setup, we implement the experiment in which the experimental results are in good agreement with the theoretical analysis results.

ACKNOWLEDGMENT

The authors acknowledge the financial support from the National Natural Science Foundation of China (Nos. 61107011 and 61077012), the Ph.D. Programs Foundation of Ministry of Education of China (No. 20123219110021) and Shanghai Aerospace Science and Technology Innovation Fund (SAST) (No. 201350).

REFERENCES

1. T. B. Pittman, Y. H. Shih, D. V. Strekalov, and A. V. Sergienko, "Optical imaging by means of two-photon quantum entanglement," *Phys. Rev. A* **52**, 3429-3432 (1995).
2. R. S. Bennink, S. J. Bentley, and R. W. Boyd, "Two-photon coincidence imaging with a classical source," *Phys. Rev. Lett.* **89**, 113601 (2002).
3. A. Gatti, E. Brambilla, M. Bache, and L. A. Lugiato, "Ghost imaging with thermal light: comparing entanglement and classical correlation," *Phys. Rev. Lett.* **93**, 93602 (2002).
4. A. Valencia, G. Scarcelli, M. D'Angelo, and Y. Shih, "Two-photon imaging with thermal light," *Phys. Rev. Lett.* **94**, 063601 (2005).
5. F. Ferri, D. Magatti, A. Gatti, and M. Bache, "High-resolution ghost image and ghost diffraction experiments with thermal light," *Phys. Rev. Lett.* **94**, 183602 (2005).
6. L. Basano and P. Ottolengo, "Experiment in lensless ghost imaging with thermal light," *Appl. Phys. Lett.* **89**, 091109 (2006).
7. F. Ferri, D. Magatti, V. G. Sala, and A. Gatti, "Longitudinal coherence in thermal ghost imaging," *Appl. Phys. Lett.* **92**, 261109 (2008).
8. Y. Bromberg, O. Katz, and Y. Silberberg, "Ghost imaging with a single detector," *Phys. Rev. A* **79**, 053840 (2009).
9. R. Meyers, K. S. Deacon, and Y. Shih, "Ghost-imaging experiment by measuring reflected photons," *Phys. Rev. A* **77**, 041801(R) (2008).
10. O. Katz, Y. Bromberg, and Y. Silberberg, "Compressive ghost imaging," *Appl. Phys. Lett.* **95**, 131110 (2009).
11. P. Zerom, K. Wai, C. Chan, and J. C. Howell, "Entangled-photon compressive ghost imaging," *Phys. Rev. A* **84**, 061804(R) (2011).
12. V. Katkovnik and J. Astola, "Compressive sensing computational ghost imaging," *J. Opt. Soc. Am. A* **29**, 1556-1567 (2012).
13. J. Cheng, "Ghost imaging through turbulent atmosphere," *Opt. Express* **17**, 7916-7921 (2009).
14. M. Bina, D. Magatti, and M. Molteni, "Backscattering differential ghost imaging in turbid media," *Phys. Rev. Lett.* **110**, 083901 (2013).
15. F. Ferri, D. Magatti, and L. A. Lugiato, "Differential ghost imaging," *Phys. Rev. Lett.* **104**, 253603 (2010).
16. B. I. Erkmen and J. H. Shapiro, "Signal-to-noise ratio of Gaussian-state ghost imaging," *Phys. Rev. A* **79**, 023833 (2009).
17. D. Magatti, A. Gatti, and F. Ferri, "Three-dimensional coherence of light speckles: Experiment," *Phys. Rev. A* **79**, 053831 (2009).
18. A. Gatti, D. Magatti, and F. Ferri, "Three-dimensional coherence of light speckles: Theory," *Phys. Rev. A* **78**, 063806 (2008).